Prediction of fatigue crack growth under constant amplitude loading and a single overload based on elasto-plastic crack tip stresses and strains

A.H. Noroozi *, G. Glinka, S. Lambert

Department of Mechanical Engineering, University of Waterloo, Waterloo, Canada N2L 3G1

Abstract

It is generally accepted that the fatigue crack growth (FCG) depends mainly on the stress intensity factor range (ΔK) and the maximum stress intensity factor (K_{max}). The two parameters are usually combined into one expression called often as the driving force and many various driving forces have been proposed up to date. The driving force can be successful as long as the stress intensity factors are appropriately correlated with the actual elasto-plastic crack tip stress–strain field. However, the correlation between the stress intensity factors and the crack tip stress–strain field is often influenced by residual stresses induced in due course.

A two-parameter (ΔK_{tot}, $K_{max,tot}$) driving force based on the elasto-plastic crack tip stress–strain history has been proposed. The applied stress intensity factors (ΔK_{appl}, $K_{max,appl}$) were modified to the total stress intensity factors (ΔK_{tot}, $K_{max,tot}$) in order to account for the effect of the local crack tip stresses and strains on fatigue crack growth. The FCG was predicted by simulating the stress–strain response in the material volume adjacent to the crack tip and estimating the accumulated fatigue damage. The fatigue crack growth was regarded as a process of successive crack re-initiations in the crack tip region. The model was developed to predict the effect of the mean and residual stresses induced by the cyclic loading. The effect of variable amplitude loadings on FCG can be also quantified on the basis of the proposed model. A two-parameter driving force in the form of: $\Delta \kappa = K_{max,tot}^{p} \Delta K_{tot}^{(1-p)}$ was derived based on the local stresses and strains at the crack tip and the Smith–Watson–Topper (SWT) fatigue damage parameter: $D = \sigma_{max} \Delta \varepsilon / 2$. The effect of the internal (residual) stress induced by the reversed cyclic plasticity manifested itself in the change of the resultant (total) stress intensity factors controlling the fatigue crack growth.

The model was verified using experimental fatigue crack growth data for aluminum alloy 7075-T6 obtained under constant amplitude loading and a single overload.
© 2007 Elsevier Ltd. All rights reserved.

Keywords: Two-parameter driving force; Fatigue crack growth; Stress ratio; Driving force; Single overload

---

* Corresponding author. Tel.: +1 519 888 4567x32346; fax: +1 519 888 6197.
  E-mail address: hnoroozi@uwaterloo.ca (A.H. Noroozi).

Nomenclature

a	crack length
b	fatigue strength exponent
c	fatigue ductility exponent
C	fatigue crack growth constant
D	fatigue damage
E	modulus of elasticity
K'	cyclic strength coefficient
M_1, M_2, M_3	weight function parameters
$m(x,a)$	weight function
m	Paris's equation exponent
N_f	number of cycle to fail the first elementary material block
P	the unit point force
n'	cyclic strain hardening exponent
p	driving force constant
R	stress ratio
R_{appl}	applied stress ratio
x	distance from the crack tip
Y	geometrical stress intensity correction factor
da/dN	crack growth rate
FCG	fatigue crack growth
SIF	stress intensity factor
SWT	Smith–Watson–Topper fatigue damage parameter
γ	fatigue crack growth equation exponent
ρ^*	notch tip radius or elementary material block size
v	Poisson's coefficient
σ'_f	fatigue strength coefficient
ε'_f	fatigue ductility coefficient
$\tilde{\varepsilon}^a_{max}$	maximum actual strain over the first elementary block
$\Delta\tilde{\varepsilon}^a$	actual strain range over the first elementary block
$\Delta\varepsilon$	strain range ahead of the crack tip
K	stress intensity factor
K_r	residual stress intensity factor
K_{op}	crack opening stress intensity factor
$K_{max,appl}$	maximum applied stress intensity factor
$K_{min,appl}$	minimum applied stress intensity factor
ΔK_{appl}	applied stress intensity range
ΔK_{eff}	effective stress intensity range
ΔK_{BL}	stress intensity factor range of base-line cycles
$K_{max,net}$	maximum net stress intensity factor
$K_{min,net}$	minimum net stress intensity factor
ΔK_{net}	net stress intensity range
$K_{max,tot}$	total maximum stress intensity factor
$K_{min,tot}$	total minimum stress intensity factor
ΔK_{tot}	total stress intensity range
$\Delta\kappa$	two-parameter driving force
$K_{max,th}$	maximum threshold stress intensity factor
ΔK_{th}	threshold stress intensity range
$S_{max,appl}$	maximum applied nominal (remote) stress

$S_{\min,\mathrm{appl}}$	minimum applied nominal (remote) stress
ΔS_{appl}	applied nominal (remote) stress range
$\tilde{\varepsilon}_{\max}^{e}$	maximum pseudo-elastic strain over the first elementary block
$\Delta\tilde{\varepsilon}^{e}$	pseudo-elastic strain range over the first elementary block
$\sigma_{\mathrm{r}}(x)$	residual stress distribution
$\sigma_{\max}$	maximum stress ahead of the crack tip
$\tilde{\sigma}_{\max}^{a}$	maximum actual stress over the first elementary block
$\Delta\tilde{\sigma}^{a}$	actual stress range over the first elementary block
$\tilde{\sigma}_{\max,\mathrm{net}}^{e}$	maximum net pseudo-elastic stress over the first elementary block
$\tilde{\sigma}_{\min,\mathrm{net}}^{e}$	minimum net pseudo-elastic stress over the first elementary block
$\Delta\tilde{\sigma}_{\mathrm{net}}^{e}$	net elastic pseudo-elastic stress range over the first elementary block
$\Delta\sigma_{\mathrm{th}}$	threshold stress range
$\Delta\tilde{\sigma}_{\mathrm{th}}^{a}$	actual threshold stress range over the first elementary block
$\psi_{\mathrm{y},i}$	the averaging constant corresponding to the i-th elementary block

1. Introduction

A lot of research effort throughout the last four decades has focused on fatigue crack growth and predictive models. The most often used model has been the Paris law [1] employing the stress intensity range as a single governing parameter and also the only driving force for the fatigue crack growth analysis.

$$\frac{\mathrm{d}a}{\mathrm{d}N} = C(\Delta K_{\mathrm{appl}})^{m}. \tag{1}$$

The Paris equation initiated widespread research activities aiming at possible improvements of its original form and at analytical modeling of FCG in general. It was found that the Paris expression was not capable of accounting for the stress ratio effect and the variable amplitude loading. The first model explaining the mean stress effect on the FCG was proposed by Elber [2]. He has postulated that only certain part of the loading and unloading reversals in a loading cycle was effective as far as the fatigue crack growth was concerned. Therefore, the applied stress intensity range, ΔK_{appl}, could not be the resultant driving force and it had to be modified to the effective stress intensity range, ΔK_{eff}, which was less than the applied one. The Elber idea was based on the observation of the crack tip closure phenomenon implicating that the maximum applied SIF did not change while the minimum applied SIF became equal to the opening SIF level, K_{op}. Although the crack tip closure model is very popular and widely used one, particularly in the aircraft industry, there are several limitations and difficulties when trying to correlate the postulated crack tip closure measurements with the fatigue crack growth behavior [3–7]. The measurements based on the crack tip displacements depend on the experimental techniques and the location of the measurement [3]. It was shown that the mean stress effect on the FCG at high stress ratios can not be explained by the closure model due to the absence of the crack closure [4] at high loads. Moreover, the effective stress intensity range, ΔK_{eff}, resulting from the closure model is not sufficient to correlate FCG in the near threshold region especially for aluminum alloys [5,6]. In vacuum tests, where the crack tip closure is insignificant, the FCG should be faster as compared to the air data, but experimental results [7] show the opposite. The observations stated above indicate that other factors influencing the FCG must be considered. Therefore, numerous research activities were devoted [5,6,8–10] to modify the original form of the Paris equation by introducing a two-parameter driving force combining the applied maximum SIF, $K_{\max,\mathrm{appl}}$, and the applied stress intensity range, ΔK_{appl}. The first form of the fatigue crack growth equation formulated in terms of the two-parameter was proposed by Walker [8].

$$\frac{\mathrm{d}a}{\mathrm{d}N} = C_1[(1-R)^p K_{\max,\mathrm{appl}}]^m = C_1[K_{\max,\mathrm{appl}}^{(1-p)}\Delta K_{\mathrm{appl}}^{p}]^m. \tag{2}$$

However, the available two-parameter driving force models [6,8–10] tend to be suitable for predicting fatigue crack growth only at relatively high stress ratios. In addition, they cannot model the effect of the compressive part of the load history and the variable amplitude loading.

One of the first models dealing with the FCG under variable amplitude loading was proposed by Wheeler [11]. He modified the constant amplitude growth rate by an empirical retardation parameter. The model could predict FCG retardations as long as the crack remained in the overload plastic zone. However, the retardation parameter depended on the loading history to be analyzed and had to be determined experimentally. The Willenborg model [12] was developed using the assumption that crack growth retardation was caused by compressive residual stresses induced by the overload. To calculate the resultant stress intensity factor, Willenborg used an effective stress which was the applied stress reduced by the compressive residual stress. Neither of these models could predict crack growth acceleration occurring just after the application of the overload. In addition, maximum retardation was predicted by theses models just after the application of the overload contrary to the experimental evidence. Therefore, several plasticity-induced crack closure models [13,14] for predicting fatigue crack growth under variable amplitude loading have been proposed. Among them, the most successful is the finite element supported crack closure model developed by Newman [15]. The Newman model was based on the strip yield plastic zone that was left in the wake of the advancing crack. According to that model, the plastically deformed material can cause crack closure even at tensile load levels. The fatigue crack growth rate, according to the model, needs to be calculated on a cycle by cycle basis. However, the calculation of the crack opening stress intensity factor, K_{op}, in the case of a variable amplitude loading is difficult. Moreover, it appears that the plasticity-induced closure in plane strain conditions [16] has relatively small effect on FCG behavior.

Therefore, a two-parameter fatigue crack growth model based on the analysis of the elasto-plastic strain–stress history at the crack tip has been developed to account for the mean stress and the variable amplitude loading effects.

2. Formulation of the two-parameter fatigue crack growth model

2.1. Description of the proposed model

After the development of fracture mechanics in 1960, the stress intensity factor range was proposed to use as a parameter characterizing the fatigue crack growth. However, it was later found out that FCG was controlled not only by the stress intensity factor range but also by the maximum stress intensity factor. In spite of the fact that the local stresses and strains near the crack tip are the dominant factors as far as the FCG is concerned, there has been little effort to establish a quantitative link between them and the applied stress intensity factors. Recently, Noroozi et al. [17] have formulated a two-parameter model to correlate the maximum stress intensity factor and the stress intensity range with the elasto-plastic crack tip stress–strain field. It was also necessary to address the fact that the actual correlation was significantly influenced by the residual stress induced at the crack tip by cyclic plastic deformations.

During the first loading or the first nominal stress reversal from 0 to 1 (Fig. 1a), the material near the crack tip is deformed plastically forming a monotonic plastic zone as shown in Fig. 1c. During the unloading part of the cycle (path 1–4 in Fig. 1a) the crack tip deformations are smaller than those created during the previous loading reversal. Thus, the plastic zone created during loading cannot disappear and a small portion of the plastic zone is deformed again in the reversed direction. This re-deformed part of the plastic zone is called the cyclic plastic zone (see Fig. 1d at load level 4). This plastically deformed material is left at the crack tip like an obstacle for subsequent reversals. The plastically deformed material prevents the region behind the crack tip from being closed. In other words, the fatigue crack surfaces do come into contact with each other but not just behind the crack tip, even if compressive loads are applied. This phenomenon was found experimentally [18,19] and also numerically [20,21] by the finite element method. The effect of the plastic zone presence resulting in the lack of contact behind the crack tip can be modeled by taking into account the crack tip residual stress. The crack opening behind the tip is modeled by adding symmetrically a residual stress distribution behind the crack tip analogous to that one existing ahead of the crack tip (Fig. 1e). The effect of the residual crack tip stress–strain field can be quantified in terms of the residual stress intensity factor, K_r. In order to calculate the residual stress intensity factor, K_r, it is necessary to determine the residual stress by taking into account the elasto-plastic material stress–strain response at the crack tip. The expected stress–strain response at the crack tip is shown schematically in Fig. 1b. The residual stress at the crack tip is induced by the
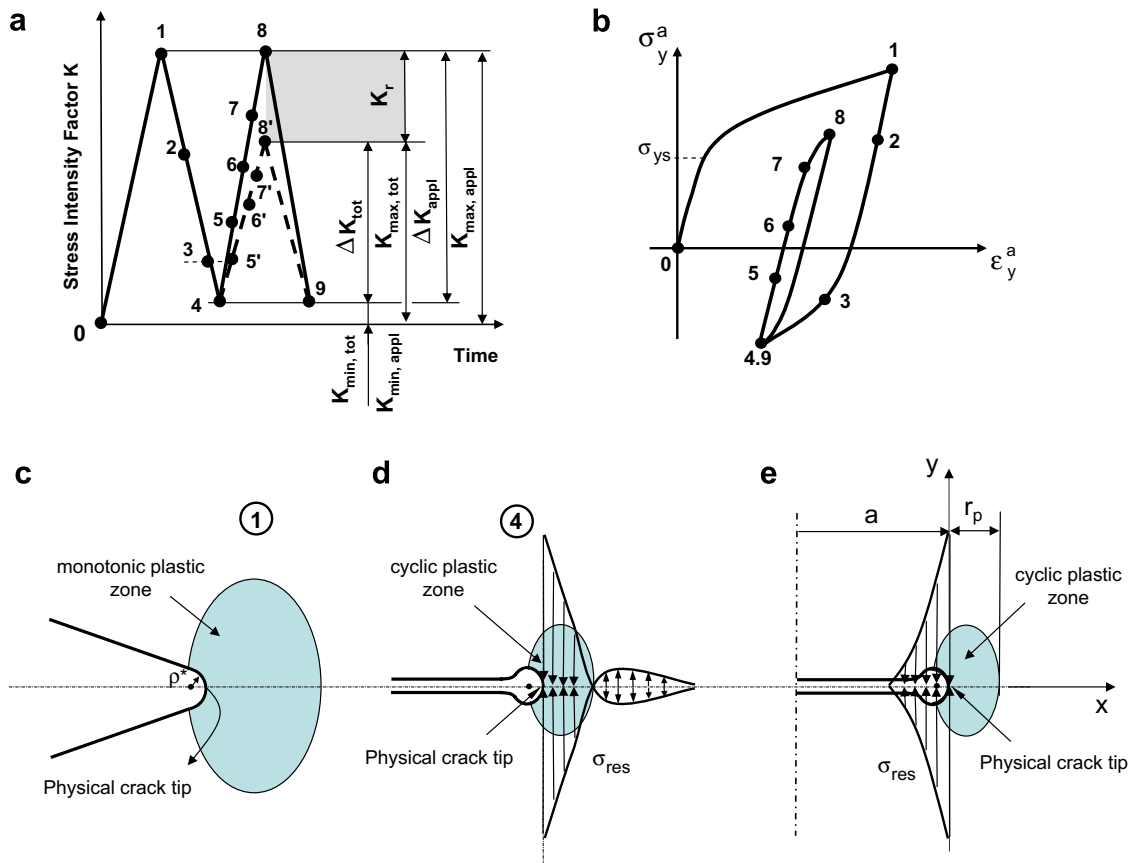
Fig. 1. Schematic crack tip geometry and qualitative crack tip stress–strain response: (a) applied load (stress intensity factor) history, (b) qualitative stress–strain response at the crack tip, (c) crack opening displacements in the crack region at maximum load level 1, (d) crack opening displacements in the crack region at minimum load level 4 and corresponding residual stresses, and (e) mathematical modeling of the crack tip region in order to simulate the effect of the residual stress field.

first two loading reversals (0–1 and 1–4, Fig. 1a). Because of the residual stress created by the first two loading reversals, the maximum stress at the crack tip corresponding to the maximum load at the end of the third reversal (at point 8 in Fig. 1a) cannot reach the same level as that one at the end of the first loading reversal (at point 1, Fig. 1a). This effect can be modeled by using the resultant maximum stress intensity factor, $K_{max,tot}$, obtained by decreasing the applied maximum stress intensity factor, $K_{max,appl}$, by the residual stress intensity factor, K_r. It is assumed that the minimum stress intensity factor is not affected by the crack tip residual stress. As a result of such a correction, both the resultant maximum stress intensity factor and the resultant stress intensity range are affected by the plasticity-induced crack tip residual stresses.

2.2. Basics of the proposed model

The proposed unified two-parameter FCG model is based on the following assumptions [17] and computational techniques:

- The material is composed of elementary particles of a finite dimension ρ^*. It represents an elementary material block size, below which the material cannot be regarded as a continuum (Fig. 2).
- The fatigue crack is regarded as a notch with the tip radius ρ^*.
- The macroscopic material properties used in the model are the Ramberg–Osgood cyclic stress–strain curve [22] and the Manson–Coffin strain–life fatigue curve [23].
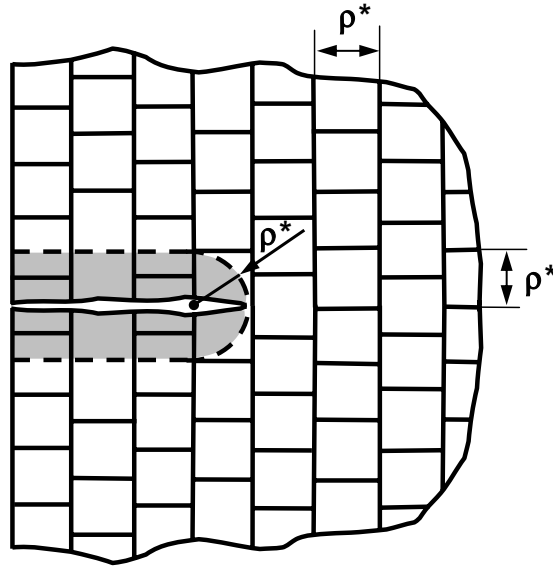
Fig. 2. The discrete material model made of elementary material blocks and the crack.

- The fatigue crack growth is considered as successive crack increments due to crack re-initiations over the distance ρ^*.
- The number of cycles N_f necessary to fail the material over the distance ρ^* can be obtained from the Manson–Coffin curve combined with the Smith–Watson–Topper (SWT) fatigue damage parameter [24].

$$D = \sigma_{\max} \frac{\Delta\varepsilon}{2} = \frac{(\sigma_f')^2}{E} (2N_f)^{2b} + \sigma_f'\varepsilon_f'(2N_f)^{b+c}. \tag{3}$$

- The fatigue crack growth rate can be finally determined as

$$\frac{\mathrm{d}a}{\mathrm{d}N} = \frac{\rho^*}{N_f}. \tag{4}$$

The mathematical formulation and stepwise computational procedure were outlined in Ref. [17] but it is also summarized below.

(1) In the case of negative stress ratios ($R < 0$), the crack was considered as a notch with the tip radius ρ^* at the maximum load level (Fig. 3 at load level 1); however, at the minimum compressive load, the crack was modeled as a circular hole (Fig. 3 at load level 2). This is due to the fact that the crack surfaces contact each other under compressive load and the load is transferred through the crack surfaces except in the region just behind the crack tip, where the crack may stay open. Therefore, the crack tip region under compressive loading can be modeled as an elliptical or circular hole. As a result, the net SIF experienced at the minimum load is not the same as it would be for a fully open crack. This way the model can account for the effect of the compressive part of a loading cycle. By modeling the crack as a circular hole under compression (Fig. 3), the minimum net SIF can be estimated from Eq. (5) discussed in detail in Ref. [17].

$$K_{\min,\mathrm{net}} = K_{\min,\mathrm{appl}} \frac{3}{2Y} \sqrt{\frac{\rho^*}{a}}. \tag{5}$$

It can be concluded, based on the proposed model, that the compressive part of a loading cycle is not very effective as far as the crack tip strain/stress concentration is concerned. Using the minimum net SIF, the net elastic stresses can be obtained from Eqs. (6)–(8) using the Creager–Paris solution [25].
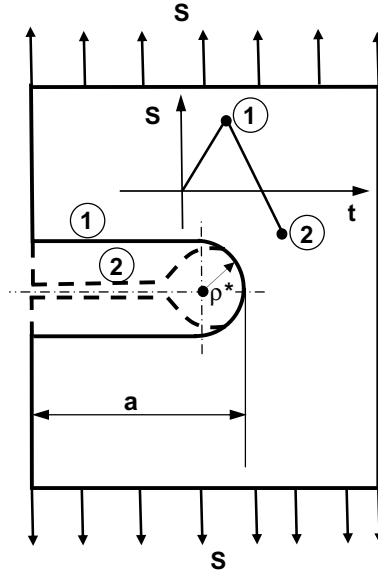
Fig. 3. The crack model (the crack opening displacement field) under the tensile maximum and compressive minimum loads used for the linear elastic stress analysis.

$$\tilde{\sigma}^{e}_{\max,net} = \frac{\psi_{y,1} K_{\max,appl}}{\sqrt{2\pi\rho^{*}}} = \frac{\psi_{y,1} S_{\max,appl} Y \sqrt{\pi a}}{\sqrt{2\pi\rho^{*}}} = S_{\max,appl} Y \sqrt{\frac{a}{2\rho^{*}}} \psi_{y,1}, \tag{6}$$

$$\sigma^{e}_{\min,net} = \frac{\psi_{y,1} K_{\min,net}}{\sqrt{2\pi\rho^{*}}} = \frac{3\psi_{y,1}}{2\sqrt{2}} \frac{K_{\min,appl}}{Y\sqrt{\pi a}} = S_{\min,appl} \frac{3\psi_{y,1}}{2\sqrt{2}}, \tag{7}$$

$$\Delta\tilde{\sigma}^{e}_{net} = \tilde{\sigma}^{e}_{\max,net} - \tilde{\sigma}^{e}_{\min,net} = \frac{\psi_{y,1}}{\sqrt{2\pi\rho^{*}}} \left(K_{\max,appl} - \frac{3}{2Y} \sqrt{\frac{\rho^{*}}{a}} K_{\min,appl} \right). \tag{8}$$

According to Eqs. (6)–(8), the maximum net stress, $\tilde{\sigma}^{e}_{\max,net}$, is the same as that one resulting from the maximum applied SIF, $K_{\max,appl}$, but the minimum net stress, $\tilde{\sigma}^{e}_{\min,net}$, can not be directly calculated by using the Creager–Paris expression. The contribution of the compressive part of the applied stress reversal (from 0 to $K_{\min,appl}$) to the local crack tip stress range is relatively small and it depends on the crack tip radius ρ^{*} and the crack size "a". It is possible that the modeling of the crack tip as a circular hole (Fig. 3) is non-conservative. In other words, the modeling of the crack tip as an elliptical hole leading to a higher stress concentration factor might be necessary in order to determine the minimum net crack tip stress, $\tilde{\sigma}^{e}_{\min,net}$, and corresponding the minimum net SIF, $K_{\min,net}$.

(2) In the case of positive stress ratios ($R \geqslant 0$), the crack was modeled as a notch with the tip radius ρ^{*} under both maximum and minimum load levels. Therefore, the elastic stresses over the first elementary material block can be calculated by using the Creager–Paris solution [25] for a crack with the tip radius ρ^{*}.

$$\tilde{\sigma}^{e}_{\max,net} = \tilde{\sigma}^{e}_{\max,appl} = \frac{\psi_{y,1} K_{\max,,\,appl}}{\sqrt{2\pi\rho^{*}}} = \frac{\psi_{y,1} S_{\max,appl} Y \sqrt{\pi a}}{\sqrt{2\pi\rho^{*}}} = S_{\max,appl} Y \sqrt{\frac{a}{2\rho^{*}}} \psi_{y,1}, \tag{9}$$

$$\tilde{\sigma}^{e}_{\min,net} = \tilde{\sigma}^{e}_{\min,appl} = \frac{\psi_{y,1} K_{\min,appl}}{\sqrt{2\pi\rho^{*}}} = \frac{\psi_{y,1} S_{\min,appl} Y \sqrt{\pi a}}{\sqrt{2\pi\rho^{*}}} = S_{\min,appl} Y \sqrt{\frac{a}{2\rho^{*}}} \psi_{y,1}, \tag{10}$$

$$\Delta\tilde{\sigma}^{e}_{net} = \Delta\tilde{\sigma}^{e}_{appl} = \frac{\psi_{y,1} K_{\max,appl}}{\sqrt{2\pi\rho^{*}}} - \frac{\psi_{y,1} K_{\min,appl}}{\sqrt{2\pi\rho^{*}}} = \frac{\psi_{y,1}}{\sqrt{2\pi\rho^{*}}} \Delta K_{appl} = \Delta S_{appl} Y \sqrt{\frac{a}{2\rho^{*}}} \psi_{y,1}, \tag{11}$$

where $S_{\min,appl} = \frac{K_{\min,appl}}{Y\sqrt{\pi a}}$, $S_{\max,appl} = \frac{K_{\max,appl}}{Y\sqrt{\pi a}}$, $\Delta S_{appl} = \frac{\Delta K_{appl}}{Y\sqrt{\pi a}}$, $\psi_{y,1} = 1.633$.

It can be seen from Eqs. (9)–(11) that the net stresses are the same as those calculated directly from the applied stress intensity factors, $K_{max,appl}$ and $K_{min,appl}$.

Finally, these elastic stresses (Eqs. (6)–(11)) can be used as the input into Neuber's rule [26] or the ESED method [27] in order to estimate actual elasto-plastic stresses and strains not only at the notch tip but also ahead of the crack (across the plastic zone), as explained in Refs. [28,29].

(3) The actual elasto-plastic stresses and strains are determined by using the above derived net stresses and the Neuber rule [26] over a number of material blocks ahead of the crack tip. The stress state over the first elementary material block is uni-axial if the body is in plane stress state. Therefore, the uni-axial Neuber rule and the Ramberg–Osgood in the form of Eqs. (12) and (13) can be used for loading and unloading reversal, respectively.

$$
\begin{cases}
\tilde{\sigma}^{e}_{max,net} \cdot \tilde{\varepsilon}^{e}_{max} = \dfrac{1}{E}\left(\dfrac{K_{max,net} \times \psi_{y,1}}{\sqrt{2\pi\rho^{*}}}\right)^{2} = \dfrac{\left(\tilde{\sigma}^{a}_{max}\right)^{2}}{E} + \tilde{\sigma}^{a}_{max}\left(\dfrac{\tilde{\sigma}^{a}_{max}}{K'}\right)^{\frac{1}{n'}}, \\[4mm]
\tilde{\varepsilon}^{a}_{max} = \dfrac{\tilde{\sigma}^{a}_{max}}{E} + \left(\dfrac{\tilde{\sigma}^{a}_{max}}{K'}\right)^{\frac{1}{n'}},
\end{cases}
\tag{12}
$$

$$
\begin{cases}
\Delta\tilde{\sigma}^{e}_{net} \cdot \Delta\tilde{\varepsilon}^{e} = \dfrac{1}{E}\left(\dfrac{\Delta K_{net} \times \psi_{y,1}}{\sqrt{2\pi\rho^{*}}}\right)^{2} = \dfrac{(\Delta\tilde{\sigma}^{a})^{2}}{E} + 2(\Delta\tilde{\sigma}^{a})\left(\dfrac{\Delta\tilde{\sigma}^{a}}{2K'}\right)^{\frac{1}{n'}}, \\[4mm]
\dfrac{\Delta\tilde{\varepsilon}^{a}}{2} = \dfrac{\Delta\tilde{\sigma}^{a}}{2E} + \left(\dfrac{\Delta\tilde{\sigma}^{a}}{2K'}\right)^{\frac{1}{n'}}.
\end{cases}
\tag{13}
$$

The actual maximum stress (Eq. (12)) and the stress range (Eq. (13)) can subsequently be used to determine the residual stress over the "first" element ahead of the crack tip. However, for other elements ahead of the crack tip, the stress state is bi-axial. Therefore, the multi-axial Neuber rule [30] and the Hencky equations of the total deformation theory of plasticity [31] were used for calculating the elasto-plastic stresses and strains over each elementary material block.

(4) The residual stress field induced by the loading and unloading stress reversals was found by subtracting the stress range, $\Delta\tilde{\sigma}^{a}$, from the maximum stress, $\tilde{\sigma}^{a}_{max}$, at several locations ahead of the crack tip resulting in a distribution of the residual stress vs. the distance from the crack tip. In order to subsequently simulate the character of the displacement field around the crack tip, the compressive residual stress field was applied behind the crack tip, as shown in Fig. 1e. The stress field was determined by applying mirror stress distribution to that one ahead of the crack tip.

(5) The residual stress effect was quantified by the residual stress intensity factor, K_r, determined by using the weight function [32] method.

$$
K_r = \int_0^a \sigma_r(x)m(x,a)\,dx,
\tag{14}
$$

where $\sigma_r(x)$ is the residual stress distribution shown in Fig. 1e and $m(x,a)$ is the universal weight function (15).

$$
m(x,a) = \dfrac{2P}{\sqrt{2\pi(a-x)}}\left[1 + M_1\left(1-\dfrac{x}{a}\right)^{\frac{1}{2}} + M_2\left(1-\dfrac{x}{a}\right)^{1} + M_3\left(1-\dfrac{x}{a}\right)^{\frac{3}{2}}\right].
\tag{15}
$$

The factors M_1, M_2 and M_3 are dependent on the specimen geometry and are given in Refs. [32,33].

3. Total stress intensity factors, $K_{max,tot}$ and ΔK_{tot}

After calculating the residual stress intensity factor, K_r, it is necessary to modify the applied stress intensity factors $K_{max,appl}$ and ΔK_{appl} in order to account for the effect of the residual stress on the fatigue crack growth. The interactions between the stress intensity factor, the plastic zone and the residual stress manifest themselves through the change (decrease) of the resultant maximum stress intensity factor, $K_{max,tot}$, without significant changes in the resultant minimum stress intensity factor, $K_{min,tot}$ (Fig. 1a). It is assumed that the residual stress

intensity factor, K_r, contributes mainly by changing (decrease) the resultant (total) maximum stress intensity factor, $K_{max,tot}$, and subsequently by the decrease of the resultant stress intensity range, ΔK_{tot}. It should be noted that the magnitude of the residual stress effect depends on the applied stress ratio and it has to be treated differently for positive and negative stress ratios, R.

3.1. Calculation of total stress intensity factors at positive stress ratios, $R_{appl} \geqslant 0$

The reversed plastic deformations around the crack tip induced at relatively high stress ratios ($R_{appl} > 0.5$) and relatively small stress intensity ranges (near threshold FCG), are usually not sufficient to produce compressive residual stresses at the crack tip. Therefore, the residual stress intensity factor is close to zero ($K_r = 0$) and the total SIFs are the same as the applied ones:

$$K_{max,tot} = K_{max,net} = K_{max,appl}, \tag{16}$$

$$K_{min,tot} = K_{min,net} = K_{min,appl}, \tag{17}$$

$$\Delta K_{tot} = \Delta K_{net} = \Delta K_{appl}. \tag{18}$$

However, at positive stress ratios $0 \leqslant R_{appl} \leqslant 0.5$ (medium range FCG rates) or at relatively high stress ratios ($R_{appl} > 0.5$) and high FCG rates the residual stresses at the crack tip can change the effectiveness of applied SIFs. The maximum total stress intensity factor, $K_{max,tot}$, is calculated in such a case by adding the negative residual stress intensity factor, K_r, to the maximum applied stress intensity factor, $K_{max,appl}$. The minimum total SIF, $K_{min,tot}$, is assumed to be unaffected by the residual stress and equals the applied minimum SIF, $K_{min,appl}$. In such a case, the total SIFs are calculated as:

$$K_{max,tot} = K_{max,net} + K_r = K_{max,appl} + K_r, \tag{19}$$

$$K_{min,tot} = K_{min,net} = K_{min,appl}, \tag{20}$$

$$\Delta K_{tot} = \Delta K_{appl} + K_r. \tag{21}$$

3.2. Calculation of total stress intensity factors at negative stress ratios, $R_{appl} < 0$

In the case of negative applied stress ratios $R_{appl} < 0$, the maximum total (resultant) stress intensity factor, $K_{max,tot}$, is calculated analogously as in the case of $R > 0$, i.e. the $K_{max,tot}$ is the algebraic sum of the maximum net, $K_{max,net}$, and the negative K_r residual stress intensity factor. However, the compressive part of the loading cycle is not entirely effective as far as FCG is concerned. Therefore, the minimum net stress intensity factor $K_{min,net}$, is not equal to the applied one and needs to be determined according to Eq. (5). Then, both the $K_{max,net}$ and $K_{min,net}$ are used for the calculation of the residual stress, σ_r, and subsequently the residual SIF, i.e. the K_r. All resultant (total) stress intensity quantities at negative stress ratios can be determined from Eqs. (22)–(24).

$$K_{max,tot} = K_{max,net} + K_r = K_{max,appl} + K_r, \tag{22}$$

$$K_{min,tot} = K_{min,net} = K_{min,appl} \frac{3}{2Y} \sqrt{\frac{\rho*}{a}}, \tag{23}$$

$$\Delta K_{tot} = K_{max,tot} - K_{min,tot} = K_{max,appl} + K_r - K_{min,appl} \frac{3}{2Y} \sqrt{\frac{\rho*}{a}} = \Delta K_{net} + K_r. \tag{24}$$

The total SIF range, ΔK_{tot}, and the total maximum SIF, $K_{max,tot}$, are the two main parameters used for subsequent fatigue crack growth predictions. However, they need to be combined into one driving force.

4. Fatigue crack growth and the two-parameter driving force

Noroozi et al. [17] have derived a two-parameter fatigue driving force combining the total stress intensity range, ΔK_{tot} and the total maximum stress intensity factor, $K_{max,tot}$, in the form of expression (25).

$$\Delta \kappa = K_{max,tot}^p \Delta K_{tot}^{(1-p)}. \tag{25}$$

The fatigue crack growth expression derived in Ref. [17] and incorporating the two-parameter driving force was finally presented as

$$\frac{\mathrm{d}a}{\mathrm{d}N} = C\left[(K_{\max,\mathrm{tot}})^p (\Delta K_{\mathrm{tot}})^{1-p} \right]^{\gamma}. \tag{26}$$

The parameter "p" in the driving force (25) is not constant but in some regions of the $\mathrm{d}a/\mathrm{d}N - \Delta K$ curve its variation is relatively small and it can be assumed constant in many practical applications. Two distinct regions of the $\mathrm{d}a/\mathrm{d}N$ vs. ΔK with approximately constant exponent "p" were found. The first region covers the fatigue crack growth regime, where plastic strains dominate the crack tip strain field. The second region is concerned with the near threshold FCG, where elastic strains dominate deformations at the crack tip. It should be noted that the constant "C" and the exponent "γ" in Eq. (26) can also be derived analytically [17].

4.1. Predominantly plastic material behavior at the crack tip

In the case of the crack tip strain field dominated by plastic strains, the constants in Eq. (26) can be approximated by expressions (27).

$$C = 2\rho^* \left[\frac{(\psi_{y,1})^2}{2^{\frac{n'+3}{n'+1}} \sigma_{\mathrm{f}}' \varepsilon_{\mathrm{f}}' \pi E \rho^*} \right]^{-\left(\frac{1}{b+c}\right)}; \quad p = \frac{n'}{n'+1}; \quad \gamma = -\frac{2}{b+c}. \tag{27}$$

The plastic driving force, $K_{\max,\mathrm{tot}}^p \Delta K_{\mathrm{tot}}^{(1-p)}$, can be used to predict FCG only in the high and medium FCG-rate regime, where plastic strains dominate at the crack tip. In these regimes, the parameter "p" is almost constant and depends mainly on the cyclic strain hardening exponent of the cyclic stress–strain material curve, n'. The driving force (26) enables the analysis of FCG for various stress ratios "R" without the necessity of changing any of the constants (Eq. (27)). In other words, Eq. (26) represents a master $\mathrm{d}a/\mathrm{d}N - \Delta K$ curve valid for all R-ratios.

4.2. Predominantly elastic material behavior at the crack tip

In the case of the crack tip strain field dominated by elastic strains, the constants in Eq. (26) can be approximated by expressions (28).

$$C = 2\rho^* \left[\frac{(\psi_{y,1})^2}{4\pi\rho^* \sigma_{\mathrm{f}}'^2} \right]^{-\frac{1}{2b}}; \quad p = 0.5; \quad \gamma = -\frac{1}{b}. \tag{28}$$

The elastic driving force, $K_{\max,\mathrm{tot}}^{0.5} \Delta K_{\mathrm{tot}}^{0.5}$, can be subsequently used to predict FCG for the near threshold region (at low FCG rates) where elastic strains dominate at the crack tip. In this region, the parameter "p" is almost constant and equal to 0.5 ($p = 0.5$).

As mentioned earlier, the elastic ($p = 0.5$) and plastic $\left(p = \frac{n'}{n'+1} \right)$ driving forces can be used only for one of the two FCG regimes. In other words, these solutions (Eqs. (27) and (28)) become less accurate in the FCG regions, where both elastic and plastic strains are equally important. To predict the fatigue crack growth at any FCG rate, in the region spanning from the near threshold to the high fatigue crack growth rate regime, the concept of approximate elasto-plastic driving force with one constant "p" has been introduced. It has been observed that the maximum notch tip strains are predominantly plastic, but the subsequent strain ranges are often dominated by elastic strains. Therefore, analogous expression such as those derived above can be used but with the "p" exponent valid over the entire range of fatigue crack growth rates, i.e. from threshold up to final fracture.

4.3. Elasto-plastic material behavior at the crack tip

Eqs. (12) and (13) provide a unique relationship between the applied stress intensity factor and the actual strains and stresses at the crack tip providing, there are not any additional effects altering those equations. Unfortunately, this is true only in the case of cracks subjected to cyclic loads applied at relatively high stress

ratios, $R_{\text{appl}} > 0.5$. At low stress ratios, a compressive residual stress field is generated ahead of the crack tip and Eqs. (12) and (13) can be used only when the net maximum stress intensity factor, $K_{\text{max,net}}$, and the net stress intensity range ΔK_{net} are corrected for the effect of the residual stress σ_r. In other words, the resultant maximum SIF, $K_{\text{max,tot}}$, and the resultant SIF range, ΔK_{tot}, discussed in Section 3 must be used in those equations. Stresses and strains over the first material volume ρ^* at the crack tip induced by the total stress intensity factors, were in this case also determined using the Neuber rule, and the Ramberg–Osgood material stress–strain curve.

$$\begin{cases} \dfrac{1}{E}\left(\dfrac{K_{\text{max,tot}} \times \psi_{y,1}}{\sqrt{2\pi\rho^*}}\right)^2 = \dfrac{(\tilde{\sigma}_{\text{max}}^a)^2}{E} + \tilde{\sigma}_{\text{max}}^a \left(\dfrac{\tilde{\sigma}_{\text{max}}^a}{K'}\right)^{\frac{1}{n'}}, \\[2mm] \tilde{\varepsilon}_{\text{max}}^a = \dfrac{\tilde{\sigma}_{\text{max}}^a}{E} + \left(\dfrac{\tilde{\sigma}_{\text{max}}^a}{K'}\right)^{\frac{1}{n'}}, \end{cases} \tag{29}$$

$$\begin{cases} \dfrac{1}{E}\left(\dfrac{\Delta K_{\text{tot}} \times \psi_{y,1}}{\sqrt{2\pi\rho^*}}\right)^2 = \dfrac{(\Delta\tilde{\sigma}^a)^2}{E} + 2(\Delta\tilde{\sigma}^a)\left(\dfrac{\Delta\tilde{\sigma}^a}{2K'}\right)^{\frac{1}{n'}}, \\[2mm] \dfrac{\Delta\tilde{\varepsilon}^a}{2} = \dfrac{\Delta\tilde{\sigma}^a}{2E} + \left(\dfrac{\Delta\tilde{\sigma}^a}{2K'}\right)^{\frac{1}{n'}}. \end{cases} \tag{30}$$

It was subsequently assumed that the crack tip strain, $\tilde{\varepsilon}_{\text{max}}^a$, induced by the maximum load was predominantly plastic, while the strain range, $\Delta\tilde{\varepsilon}^a$, was predominantly elastic. After neglecting approximately the elastic and plastic terms, Eqs. (29) and (30) take the following forms:

$$\begin{cases} \dfrac{1}{E}\left(\dfrac{K_{\text{max,tot}} \times \psi_{y,1}}{\sqrt{2\pi\rho^*}}\right)^2 = \sigma_{\text{max}}^a \left(\dfrac{\tilde{\sigma}_{\text{max}}^a}{K'}\right)^{\frac{1}{n'}}, \\[2mm] \tilde{\varepsilon}_{\text{max}}^a = \left(\dfrac{\tilde{\sigma}_{\text{max}}^a}{K'}\right)^{\frac{1}{n'}}, \end{cases} \tag{31}$$

$$\begin{cases} \dfrac{1}{E}\left(\dfrac{\Delta K_{\text{tot}} \times \psi_{y,1}}{\sqrt{2\pi\rho^*}}\right)^2 = \dfrac{(\Delta\tilde{\sigma}^a)^2}{E}, \\[2mm] \dfrac{\Delta\tilde{\varepsilon}^a}{2} = \dfrac{\Delta\tilde{\sigma}^a}{2E}. \end{cases} \tag{32}$$
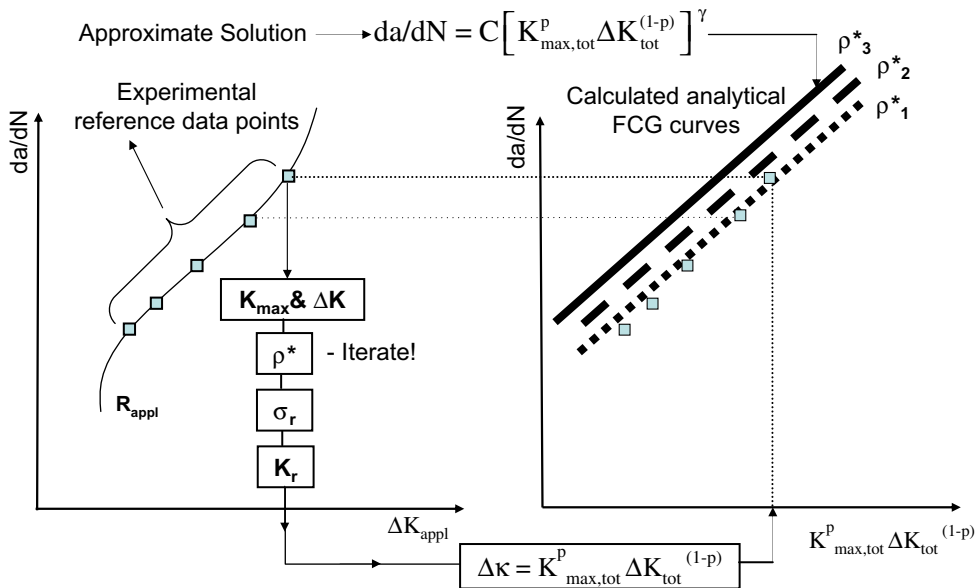

Fig. 4. The method for iterative determination of the ρ^* parameter based on high FCG experimental data obtained at arbitrary stress ratio R.
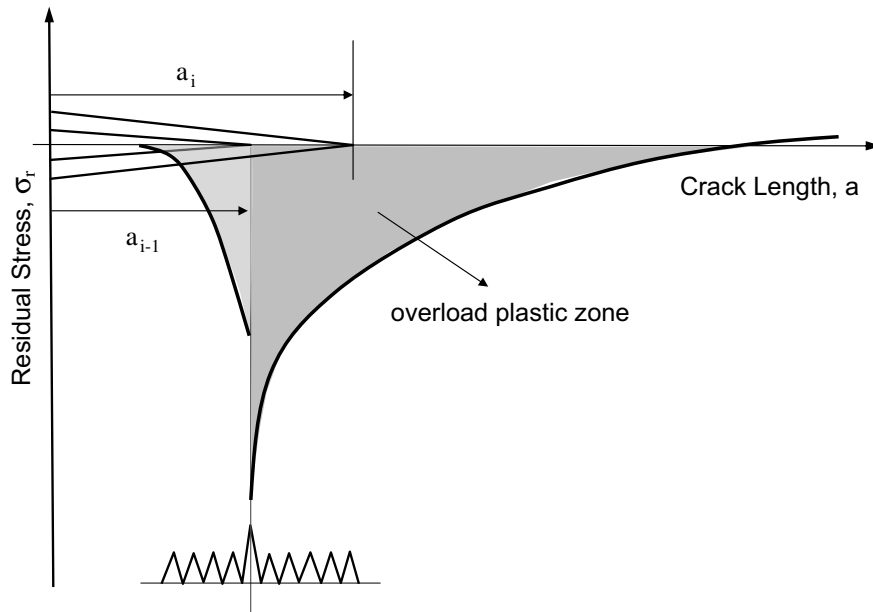
Fig. 5. Schematic of residual stress distribution used for the calculation of residual stress intensity factors after an overload.
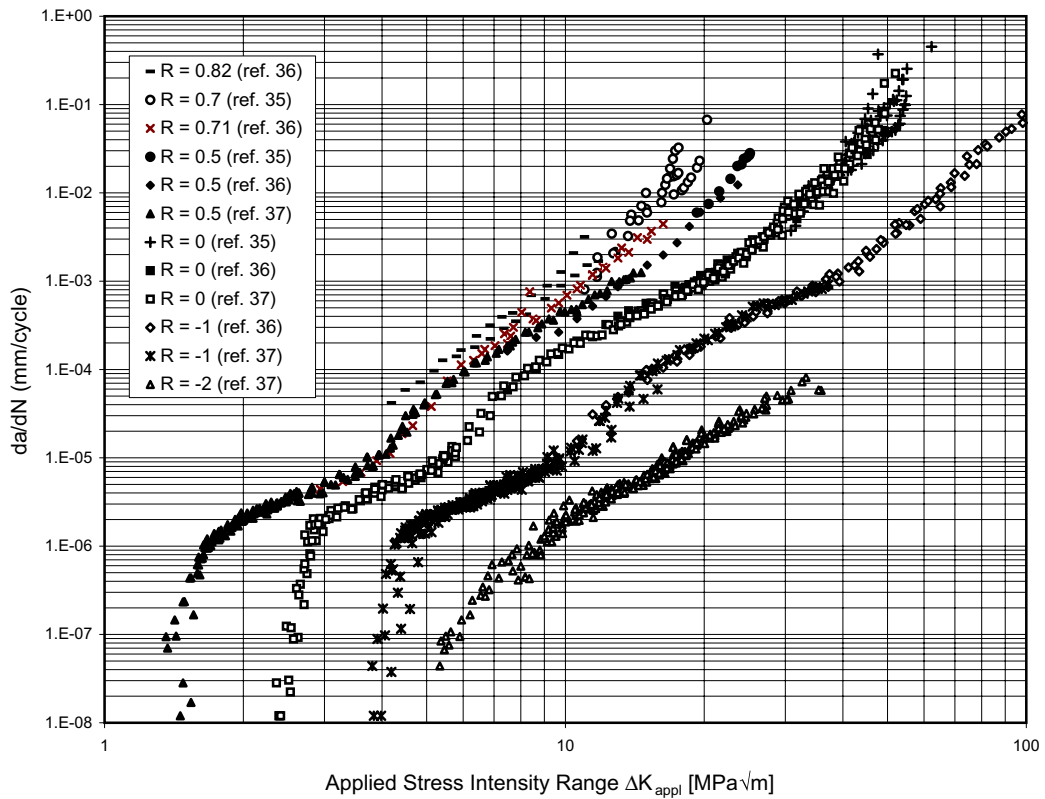

Fig. 6. Crack growth rate as a function of the applied stress intensity range, 7075-T6 Al alloy [35–37].

The plastic term in the Manson–Coffin together with the SWT parameter (Eq. (3)) was also omitted.

$$\tilde{\sigma}_{\max}^{a} \frac{\Delta \tilde{\varepsilon}^{a}}{2} = \frac{(\sigma_{f}')^{2}}{E} (2N_{f})^{2b}. \tag{33}$$

Using Eqs. (4), (31)–(33), the final FCG expression was derived in the form of Eq. (34).

$$\frac{\mathrm{d}a}{\mathrm{d}N} = C[(K_{\max,\mathrm{tot}})^{p} (\Delta K_{\mathrm{tot}})^{0.5}]^{\gamma}, \tag{34}$$

where

$$C = 2\rho^{*} \left[\frac{1}{2(\sigma_{f}')^{2}} \times \left[\left(\frac{\psi_{y,1}}{\sqrt{2\pi\rho^{*}}} \right)^{3n'+1} \times \frac{K'}{E^{n'}} \right]^{\frac{1}{n'+1}} \right]^{\frac{-1}{2b}}; \quad p = \frac{n'}{n'+1}; \quad \gamma = -\frac{1}{b}.$$

The FCG expression (34) indicate how the two SIF parameters, ΔK_{tot} and $K_{\max,\mathrm{tot}}$, characterizing the loading cycle should be combined into one driving force in the form of

$$\Delta\kappa = K_{\max,\mathrm{tot}}^{p} \Delta K_{\mathrm{tot}}^{0.5}. \tag{35}$$

It should also be noted that the driving force (35) is resulting from the application of the SWT fatigue damage parameter. All constants in the FCG equations discussed above can be obtained from the material properties given in the form of the Ramberg–Osgood stress–strain curve and the Manson–Coffin fatigue strain–life expression. The elementary material block size, ρ^{*}, must be determined separately.
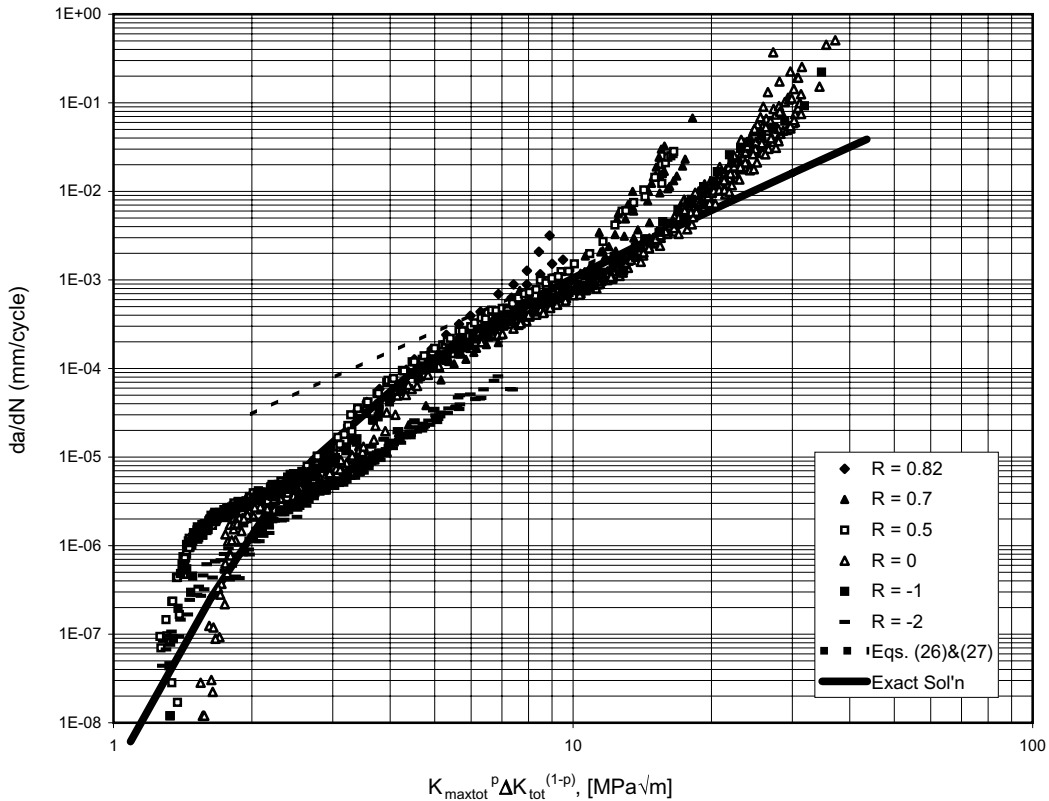

Fig. 7. Fatigue crack growth as a function of the "plastic" two-parameter driving force, $K_{\max,\mathrm{tot}}^{p} \Delta K_{\mathrm{tot}}^{(1-p)}$, 7075-T6 Al alloy.

5. Estimation of the size of the elementary material block and the crack tip radius, ρ^*

The method for estimating the parameter ρ^* depends on the nature of available experimental data. If the near threshold fatigue crack growth data at high stress ratios $R > 0.5$ is available, the determination of the crack tip radius, ρ^*, can be carried out by solving the set of simultaneous Eqs. (3), (4), (29), and (30). The total stress intensity factors, $K_{\max,\text{tot}}$ and ΔK_{tot}, have the same magnitudes at high stress ratios as the applied ones. Therefore, the applied SIFs can be used in Eqs. (29), and (30) in order to calculate the maximum stress, $\tilde{\sigma}^a_{\max}$, and the strain range, $\Delta\tilde{\varepsilon}^a$. Knowing the maximum stress, $\tilde{\sigma}^a_{\max}$, and the strain range, $\Delta\tilde{\varepsilon}^a$, the elementary material block size ρ^* can be determined from Eq. (36).

$$\tilde{\sigma}^a_{\max}\frac{\Delta\tilde{\varepsilon}^a}{2} = \frac{\left(\sigma'_{\text{f}}\right)^2}{E}\left(\frac{2\rho^*}{\mathrm{d}a/\mathrm{d}N}\right)^{2b} + \sigma'_{\text{f}}\varepsilon'_{\text{f}}\left(\frac{2\rho^*}{\mathrm{d}a/\mathrm{d}N}\right)^{b+c}. \tag{36}$$

However, because both sides of Eq. (36) depend on the ρ^* parameter, the iteration technique must be used.

If the near threshold fatigue crack growth data at high stress ratios is not available, fatigue crack growth data obtained experimentally at any stress ratio can be used for the determination of the elementary material block size ρ^*. First, the residual SIF, K_{r}, need to be determined for assumed ρ^* followed by the determination of the total stress intensity factors, $K_{\max,\text{tot}}$ and ΔK_{tot}, corresponding to given experimental FCG data. The total stress intensity factors are subsequently combined into the two-parameter driving force, $\Delta\kappa = K^p_{\max,\text{tot}}\Delta K^{(1-p)}_{\text{tot}}$. Then, the experimental fatigue crack growth data can be plotted in terms of the two-parameter driving force, $\mathrm{d}a/\mathrm{d}N$ vs. $\Delta\kappa$. Finally, by using Eqs. (26), (27) and assumed ρ^* parameter, the calculated $\mathrm{d}a/\mathrm{d}N$ vs. $\Delta\kappa$ can also be drawn (Fig. 4). If the calculated $\mathrm{d}a/\mathrm{d}N$ vs. $\Delta\kappa$ is in good agreement with the
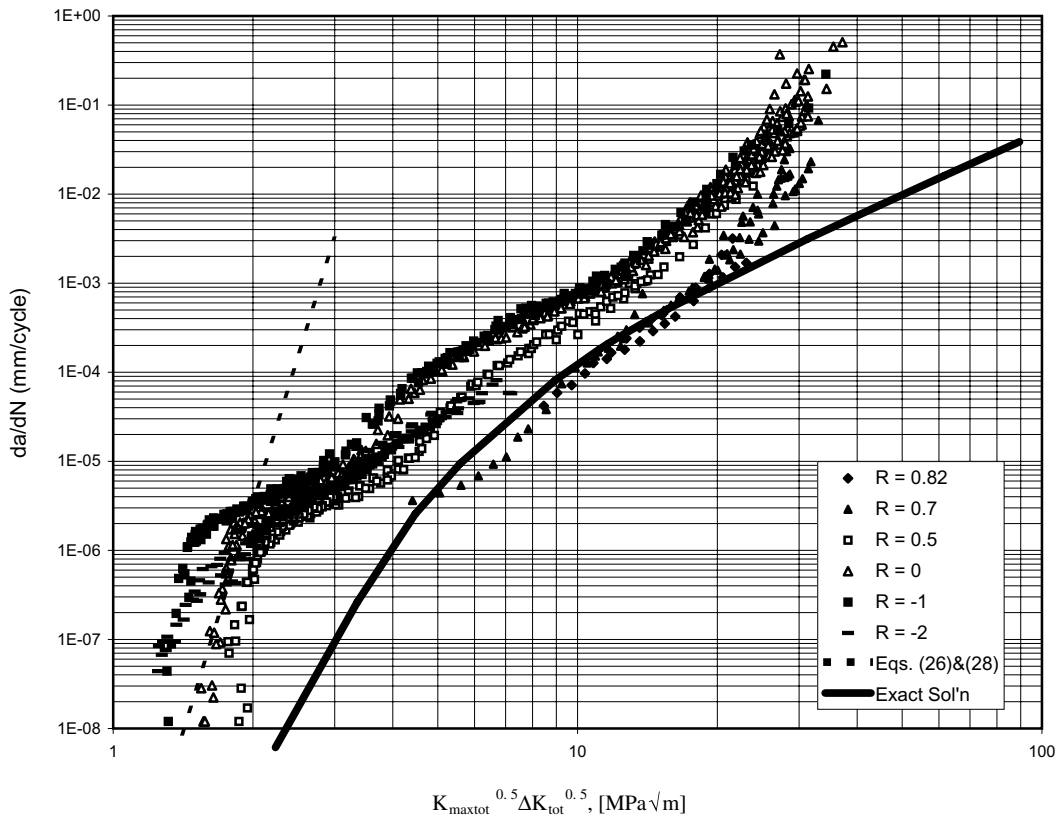

Fig. 8. Fatigue crack growth as a function of the "elastic" two-parameter driving force, $K^{0.5}_{\max,\text{tot}}\Delta K^{0.5}_{\text{tot}}$, 7075-T6 Al alloy.

experimental $\mathrm{d}a/\mathrm{d}N$ vs. $\Delta\kappa$ curve, the initial assumption concerning the ρ^* parameter was correct. The whole process needs to be iterated until the correct value of the parameter ρ^* is determined. It is recommended to use in this case the high fatigue crack growth data as the reference because the high-rate FCG is governed predominantly by plastic strains and the use of Eqs. (26) and (27) is justified.

6. Prediction of the fatigue crack growth after the application of a single overload

The interaction effects that occur under variable amplitude loading can manifest themselves in a change of the total instantaneous driving force, $\Delta\kappa$, and consequently the change of the fatigue crack growth rate. It can be assumed that the plastic zone induced by the constant amplitude loading just before the overload is applied remains in the wake of the advancing crack tip. After the overload is applied, the fatigue crack growth is influenced by the stresses induced by the overload plastic zone. A typical residual stress distribution used to calculate the residual stress intensity factors after the overload is shown in Fig. 5. The residual stress field consists of two stress fields that are not symmetric: the first one created by the base constant amplitude loading remains in the wake of the advancing crack tip; the second one was created by a single overload. As the crack is penetrating into the overload plastic zone, the magnitude of the residual stress intensity factor increases, due to the increase of the compressive residual stress, and consequently the fatigue crack growth decreases. As soon as the magnitude of the residual SIF induced by the overload stress field is the same as that one induced by the subsequent constant amplitude base loading, the overload effect is assumed to cease. In other words, beyond this point the fatigue crack growth needs to be calculated by using the residual SIF induced by the post-overload or the current load fluctuations.
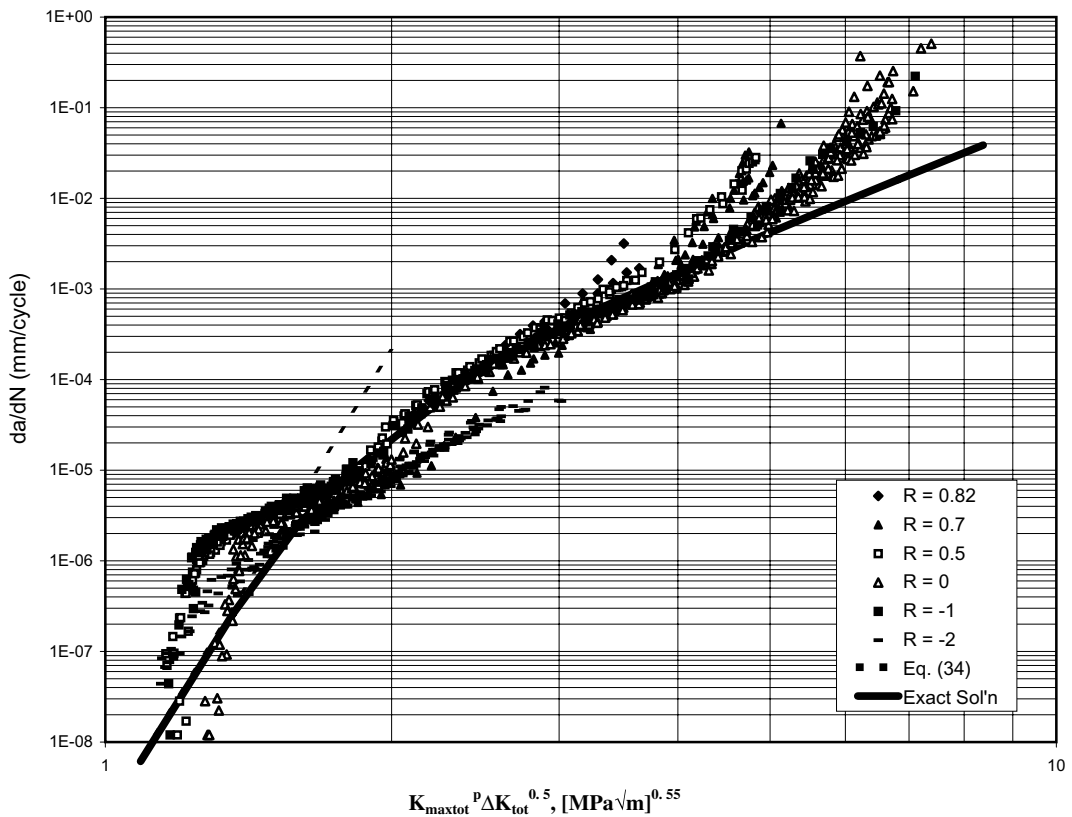

Fig. 9. Fatigue crack growth as a function of the 'mixed' two-parameter driving force, $K_{\max,\mathrm{tot}}^p \Delta K_{\mathrm{tot}}^{0.5}$, 7075-T6 Al alloy.

7. Verification of the proposed model

The fatigue crack growth data of 7075-T6 aluminum alloy was used for the validation of the proposed model. The cyclic and fatigue properties were borrowed from Ref. [34] and are listed below:

Monotonic material properties: $E = 71700$ MPa, $\sigma_{ys} = 468.85$ MPa, $v = 0.32$.
Cyclic stress–strain curve (see Eq. (12)): $K' = 737.81$ MPa, $n' = 0.056$.
Strain–life curve (see Eq. (3)): $b = -0.059$, $c = -0.802$, $\varepsilon'_f = 0.2638$, $\sigma'_f = 729.62$ MPa.

7.1. Fatigue crack growth prediction under constant amplitude loading

The experimental FCG data for the 7075-T6 aluminum alloy was found in Refs. [35–37]. The data for various R-ratios is plotted as a function of the applied stress intensity range (Fig. 6). Due to the availability of the near threshold FCG data obtained at high stress ratios, the ρ^* parameter was determined by the first method described in Section 5. The data used were: $R = 0.5$, $da/dN = 1 \times 10^{-8}$ (mm/cycle) and $\Delta K_{th} = 1.4$ (MPa$\sqrt{m}$). The size of the elementary material block was found to be $\rho^* = 4 \times 10^{-6}$ (m). All other parameters of the fatigue crack growth equations (Eqs. (26)–(28) and (34)) were as follows:

– *for predominantly plastic material behavior at the crack tip* – Eqs. (26), (27)
 $C = 6.1 \times 10^{-9}$, $p = 0.05$, $\gamma = 2.32$ (for da/dN in "mm/cycle" and K in "MPa$\sqrt{m}$"),
– *for predominantly elastic material behavior at the crack tip* – Eqs. (26), (28)
 $C = 2.61 \times 10^{-14}$, $p = 0.5$, $\gamma = 16.95$ (for da/dN in "mm/cycle" and K in "MPa$\sqrt{m}$"),
– *for mixed elastic–plastic material behavior at the crack tip* – Eq. (34)
 $C = 1.63 \times 10^{-12}$, $p = 0.05$, $\gamma = 16.95$ (for da/dN in "mm/cycle" and K in "MPa$\sqrt{m}$").
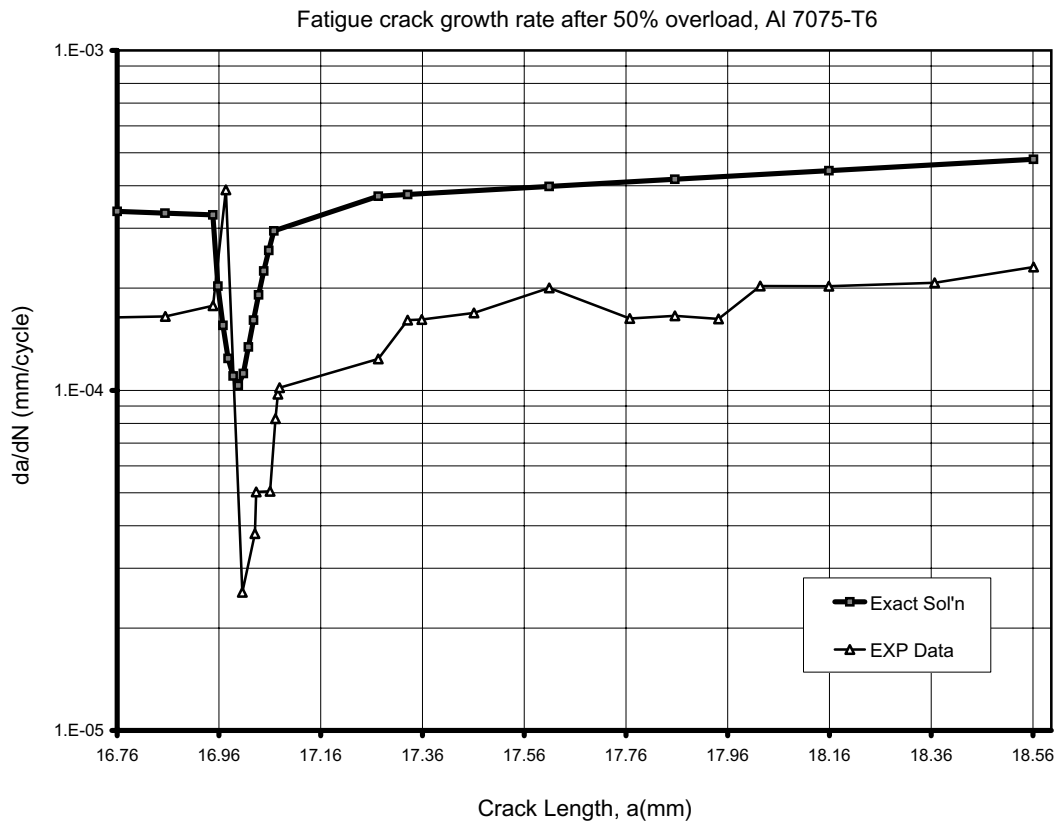

Fig. 10. Experimental and predicted fatigue crack growth rates after 50% overload (7075-T6 Al alloy, $\Delta K_{BL} = 11.4$ MPa$\sqrt{m}$).

Three two-parameter driving forces, $K_{\max,tot}^{p}\Delta K_{tot}^{(1-p)}$, $K_{\max,tot}^{0.5}\Delta K_{tot}^{0.5}$ and $K_{\max,tot}^{p}\Delta K_{tot}^{0.5}$, were used to model the effect of the stress ratio R on the fatigue crack growth under constant amplitude loading. The total stress intensity factors corrected for the residual stress effect were used to determine the magnitude of each driving force. It was found (Fig. 7) that in the high and medium FCG rate regimes, the "plastic" driving force, $K_{\max,tot}^{p}\Delta K_{tot}^{(1-p)}$, was successful in correlating the fatigue crack growth data obtained at various stress ratios. The "elastic" driving force, $K_{\max,tot}^{0.5}\Delta K_{tot}^{0.5}$, was the least successful even in the near threshold region (Fig. 8). It can be noted that the elastic driving force may be used only to consolidate FCG data at very low fatigue crack growth rates; therefore, it is not recommended to be used for fatigue crack growth predictions away from the threshold. It was also found (Fig. 9) that the combination of the elastic and plastic stress–strain material behavior at the crack tip in the form of the driving force, $K_{\max,tot}^{p}\Delta K_{tot}^{0.5}$, could be used to correlate FCG data at various R-ratios for the FCG rates spanning from the near threshold to the high growth rate regime.

The closed form solutions of Eqs. (26)–(28) and (34) were attainable after neglecting the plastic or elastic terms, respectively, in the Ramberg–Osgood and the Manson–Coffin equation. Unfortunately, such solutions become inaccurate in the regions, where both terms are equally important. However, numerical solutions to the complete set of Eqs. (3), (4), (29), and (30), i.e. without neglecting any terms, are possible to obtain. The final solution cannot be derived in a closed form but it can be presented graphically. The numerical solution is termed further on as the "exact solution". The "exact" FCG curves resulted from solving the complete set of Eqs. (3), (4), (29), and (30) are shown as diagrams (Figs. 7–9), where the fatigue crack growth rates are plotted as a function of the appropriate driving force $\Delta\kappa$. The approximate closed form solutions (Eqs. (26)–(28) and (34)), are also shown in the same figures with the dashed lines. The best results in correlating the FCG under various stress ratios were obtained while using the mixed driving force in the form of $K_{\max,\ tot}^{p}\Delta K_{tot}^{0.5}$. As shown in Fig. 9, the numerical exact solution presented in terms of the mixed driving force had good agreement with
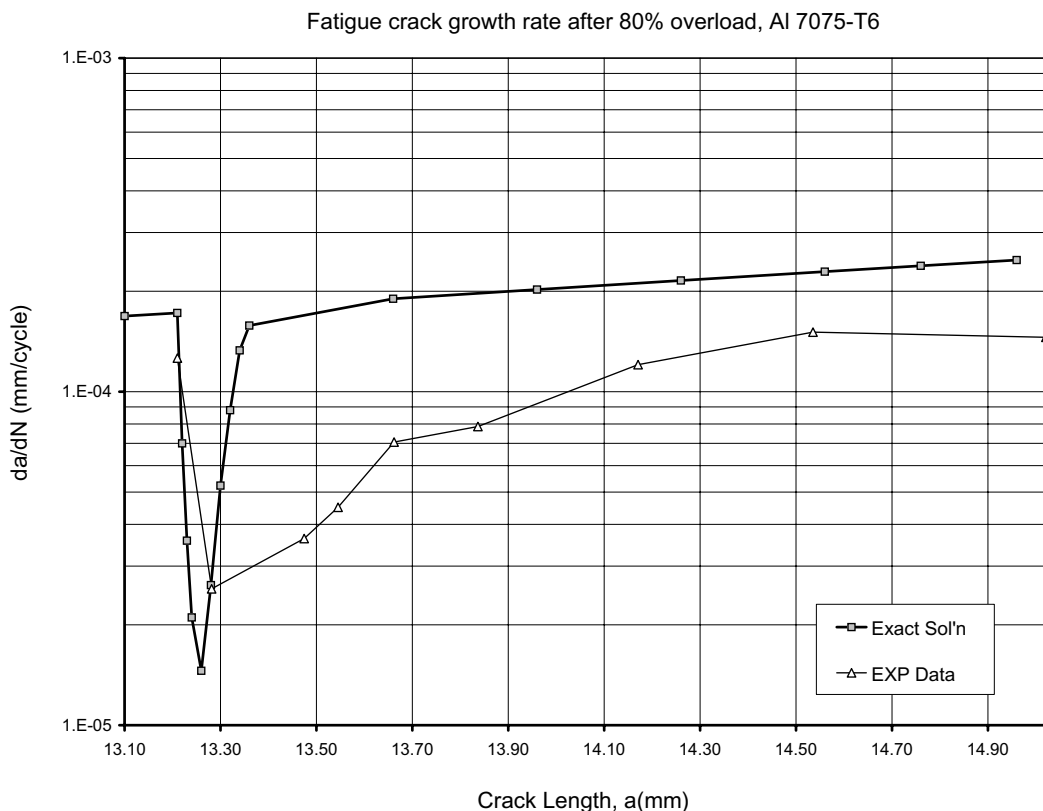

Fig. 11. Experimental and predicted fatigue crack growth rates after 80% overload (7075-T6 Al alloy, $\Delta K_{BL} = 8.955$ MPa$\sqrt{m}$).

the experimental data over the entire range of FCG data. However, the elasto-plastic approximate solution (Eq. (34)) agreed well with only the low FCG data. Therefore, it is recommended that in practice two lines da/dN vs. $\Delta\kappa$ should be fitted into the existing FCG data for the determination of constants "C" and "γ" in Eq. (34), i.e. one line covering the near threshold FCG data and the other approximating so called Paris' regime. The two power law curves characterized by two sets of constants (the exponent "γ" and the constant "C") can be subsequently used for FCG analyses.

7.2. Fatigue crack growth prediction after the application of a single overload

The proposed model was also used to predict the fatigue crack growth rate after the application of a single overload. The experimental fatigue crack growth data for the 7075-T6 aluminum alloy from Ref. [38] was used for the validation. The predicted and experimental fatigue crack growth retardation following a single overload is shown in Figs. 10 and 11. The experimental post-overload FCG rate was measured [38] in load-controlled fatigue tests on 7075-T6 aluminum alloy specimen at $R = 0.1$ with the overload ratios of 1.5 and 1.8 and the base stress intensity range $\Delta K_{BL} = 11.4$ MPa$\sqrt{m}$ and $\Delta K_{BL} = 8.955$ MPa$\sqrt{m}$, respectively. The predicted fatigue crack growth rates based on the numerical "exact" solution are also shown in Figs. 10 and 11. The discrepancy between the theoretical and experimental curves was due to the inaccuracy of the ρ^* parameter. The ρ^* parameter was estimated using one constant amplitude FCG data set from Refs. [35–37] and the predictions were carried out for another set of data borrowed from Ref. [38]. It is not certain whether the material properties of the two different sets of specimens tested at different laboratories and separated by at least a few years time span were exactly the same.

8. Conclusions

A fatigue crack growth model based on the simulation of the elastic–plastic stress–strain response at the crack tip has been proposed. The application of the model resulted in the derivation of a two-parameter driving force combining the effect of the maximum stress intensity factor and the stress intensity range. It was shown that after correcting the applied stress intensity factors for the effect of the plasticity-induced residual stresses near the crack tip it was possible to derive one master fatigue crack growth curve valid for all stress ratios.

Three forms of the fatigue crack driving force, $K_{max,tot}^p \Delta K_{tot}^{(1-p)}$, $K_{max,tot}^{0.5} \Delta K_{tot}^{0.5}$ and $K_{max,tot}^p \Delta K_{tot}^{0.5}$, were derived depending on the assumptions concerning the nature of the crack tip stress–strain field. It was shown that the driving force in the form of $K_{max,tot}^p \Delta K_{tot}^{0.5}$ could correlate FCG data for a wide range of stress ratios and FCG rates. The driving force $K_{max,tot}^p \Delta K_{tot}^{(1-p)}$ could only be used for predicting the high FCG rates. However, the driving force of $K_{max,tot}^{0.5} \Delta K_{tot}^{0.5}$ was not good for FCG predictions, even in the near threshold region.

The model was also able to account for the detrimental effect of the compressive part of a loading cycle. It was found that the contribution of the compressive part of the stress reversal was relatively small and depended on the crack tip radius, ρ^*, and the actual crack size, a. However, the modeling of the crack tip as a circular hole might be non-conservative. The model could be used to predict the fatigue crack growth after a single overload, and it can be potentially applied for analyses of FCG under spectrum loading.

Acknowledgement

References

[1] Paris PC, Erdogan F. A critical analysis of crack propagation laws. J Basic Engng 1963;D85:528–34.
[2] Elber W. The significance of fatigue crack closure. In: Damage tolerance in aircraft structure, ASTM STP 486. American Society for Testing and Materials; 1971. p. 230–42.
[3] Macha DE, Corby DM, Jones JW. On the variation of fatigue-crack-opening load with measurement location. Exp Mech 1979;19(6):207–13.
[4] Shih TT, Wei RP. A study of crack closure in fatigue. Engng Fract Mech 1974;6(1):19–32.

 [5] Kujawski D. A new $(\Delta K^+ K_{max})^{0.5}$ driving force parameter for crack growth in aluminum alloys. Int J Fatigue 2001;23(8):733–40.
 [6] Donald K, Paris PC. An evaluation of ΔK_{eff} estimation procedure on 6061-T6 and 2024-T3 aluminum alloys. Int J Fatigue 1999;21(S1):47–57.
 [7] Kirby BR, Beevers CJ. Slow fatigue crack growth and threshold behavior in air and vacuum of commercial aluminum alloys. Fatigue Engng Mater Struct 1979;1(2):203–15.
 [8] Walker EK. The effect of stress ratio during crack propagation and fatigue for 2024-T3 and 7075-T6 aluminum. In: Effect of environment and complex load history on fatigue life, ASTM STP 462, American Society for Testing and Materials; 1970. p. 1–14.
 [9] Vasudevan AK, Sadananda K, Louat N. A review of crack closure, fatigue crack threshold and related phenomena. Mater Sci Engng 1994;A188(1–2):1–22.
[10] Dinda S, Kujawski D. Correlation and prediction of fatigue crack growth for different R-ratios using K_{max} and ΔK^+ parameters. Engng Fract Mech 2004;71(12):1779–90.
[11] Wheeler OE. Spectrum loading and crack growth. Trans ASME, J Basic Engng 1972;94(1):181–6.
[12] Willenborg J, Engle RM, Wood HA. A crack growth retardation model using an effective stress concept. Report No. AFFDL TM-71-1- FBR, USAF. Air Force Flight Dynamic Laboratory; 1971.
[13] De Koning AU. A simple crack closure model for prediction of fatigue crack growth rates under variable-amplitude loading. In: Roberts R, editor. Fract Mech, ASTM STP 743. American Society for Testing and Materials; 1981. p. 63–85.
[14] Padmadinata UH. Investigation of crack-closure prediction models for fatigue in aluminum alloy sheet under flight-simulation loading. Report LR-619. Delft University of Technology, Faculty of Aerospace Engineering; 1990.
[15] Newman JR. Prediction of fatigue crack growth under variable–amplitude and spectrum loading using a closure model. In: Abelkis PR, Hudson CM, editors. Design of fatigue and fracture resistant structure, ASTM STP 761. American Society for Testing and Materials; 1982. p. 255–77.
[16] McEvily AJ, Yang Z. In: Czoboly E, editor. Failure analysis – theory and practice. Warley, UK: Engineering Materials Advisory Services; 1988. p. 1231–48.
[17] Noroozi AH, Glinka G, Lambert S. A two parameter driving force for fatigue crack growth analysis. Int J Fatigue 2005;27(10–12):1277–96.
[18] Bowles CQ. The role of environment, frequency, and shape during fatigue crack growth in aluminum alloys. Doctoral Dissertation. Delft University, The Netherlands; 1978.
[19] Jones R. Private communications. DSTO Centre for Structural Mechanics, Department of Mechanical Engineering, Monash University, Victoria, Australia; 2006.
[20] Pommier S. A study of the relationship between variable level fatigue crack growth and the cyclic constitutive behavior of steel. Int J Fatigue 2001;23(S1):111–8.
[21] Sander M, Richard HA. Lifetime prediction for real loading situations-concepts and experimental results of fatigue crack growth. Int J Fatigue 2003;25(9–11):999–1005.
[22] Ramberg W, Osgood WR. Description of stress–strain curves by three parameters. NACA Technical Note No. 902. Notational Advisory Committee for Aeronautics; 1943.
[23] Tavernelli JF, Coffin LF. Experimental support for generalized equation predicting low cycle fatigue, and Manson SS. Discussion. Trans ASME, J Basic Engng 1962;84(4):533–41.
[24] Smith KN, Watson P, Topper TH. A stress–strain function for the fatigue of metals. J Mater 1970;5(4):767–78.
[25] Creager M, Paris PC. Elastic field equations for blunt cracks with reference to stress corrosion cracking. Int J Fract Mech 1967;3(4):247–52.
[26] Neuber H. Theory of stress concentration for shear-strained prismatic bodies with arbitrary nonlinear stress–strain law. Trans ASME, J Appl Mech 1961;28:544–51.
[27] Molski K, Glinka G. A method of elastic–plastic stress and strain calculation at a notch root. Mat Sci Engng 1981;50(1):93–100.
[28] Glinka G, ott W, Nowack H. Elastoplastic plane strain analysis of stresses and strains at the notch root. J Engng Mater Technol Trans ASME 1988;110(3):195–204.
[29] Glinka G. Relations between the strain energy density distribution and elastic–plastic stress–strain fields near cracks and notches and fatigue life calculation. In: Slomon HD, Halford GR, Kaisand LR, Leis BN, editors. Low cycle fatigue, ASTM STP 942. American Society for Testing and Materials; 1988. p. 1022–47.
[30] Glinka G, Buczynski A. In: Kalluri S et al. editors. Multi-axial fatigue and deformation, ASTM STP 1387. American Society for Testing and Materials; 2000. p. 82–98.
[31] Skrzypek JJ, Hetnarski RB. Plasticity and creep: theory, examples and problems. Boca Raton: CRC Press; 1993.
[32] Shen G, Glinka G. Determination of weight functions from reference stress intensity factor. Theor Appl Fract Mech 1991;15(3):237–45.
[33] Wang X, Lambert S, Glinka G. Approximate weight functions for embedded elliptical cracks. Engng Fract Mech 1998;59(3):381–92.
[34] Jiang Y. Private communications. Department of Mechanical Engineering, University of Nevada, Reno; 2005.
[35] Dubensky RG. Fatigue crack propagation in 2024-T3 and 7075-T6 aluminum alloys at high stress. Report No. NASA CR–1732; 1971.
[36] Hudson CM. Effect of stress ratio on fatigue crack growth in 7075-T6 and 2024-T3 aluminum alloy specimens. Report No. NASA TN D-5390; 1969.
[37] Newman JC, Wu X R, Venneri SL, Li CG. Small-crack effects in high strength aluminum alloys – A NASA/CAE cooperative program. NASA Reference Publication 1309; 1994.
[38] Chanani GR. Retardation of fatigue-crack growth in 7075 aluminum. Met Engng Quart 1975;5(1):40–8.